SIMULATION OF THE DUCTILE BEHAVIOR OF ROCK SALT

Geovani Bresolin, geovani_bresolin@yahoo.com.br
Marcelo Krajnc Alves, krajnc@emc.ufsc.br
Department of Mechanical Engineering, Federal University of Santa Catarina, Florianópolis, Brazil

Hazim Ali Al-Qureshi, alhazim@emc.ufsc.br
Department of Material Engineering, Federal University of Santa Catarina, Florianópolis, Brazil

Abstract. *The objective of this work is to present a viscoplastic model and to propose and implement an implicit algorithm, using the Galerkin Finite Element Method, for the analysis of the ductile behavior of rock salt. The ductile behavior of rock salt is observed under deepwater oil field developments, in which the rock salt is subjected to large confining pressures. The model considered in this work takes into account a work hardening phenomenon, a dynamic and static recovery mechanism, and the additive decomposition of the stress tensor into an active and an inactive part. The inactive part of the stress tensor is given as the sum of a short term and a long term effect making the model adequate for modeling the behavior of rock salt under arbitrary loading. A continuous consistent tangent operator is derived by a proper linearization of the weak form of the equilibrium equation. For simplicity, one considers only plane strain and axisymmetric problems and employs a Tri6 finite element in order to avoid volumetric locking phenomena. In order to attest the adequacy of the proposed algorithm and to verify the robustness of the developed software one considers the solution of a triaxial compression test, a creep test, a relaxation test and a type of indirect traction test, employed for the indirect determination of the tension strength of rock salt.*

Keywords*: viscoplasticity, rock salt, finite elements*

1. INTRODUCTION

Initially, the objective is to give a general view of the behavior of rock salt. Natural rock salt is polycrystalline and exhibits a deformation behavior that is similar to the deformation behavior of rocks in the brittle regime and of metals in the ductile regime. It creeps under any deviatory stress. For mean (hydrostatic) stresses typically less than 5 *MPa* it will dilate with time, upon application of a deviatory stress. However, it will flow with constant volume above a mean stress of approximately 5 *MPa*. The creep response of salt involves either two or three stages. For confining pressures typically less than 5 *MPa*, salt specimens subjected to a constant stress state will creep through three stages. In the first stage, named primary creep, the strain rate begins with a very high rate and decreases to a constant rate, due to work hardening. In the secondary creep stage, named steady creep stage, the specimen deforms at approximately a constant strain rate. In the third stage (tertiary creep) the strain rate increases until failure occurs as a result of the nucleation of micro voids and micro cracks associated with a damage process. Now, for confining pressures typically above 5 *MPa*, only the primary and secondary stages are evident from experimental tests. In the particular case of deepwater oil field developments, the confining mean (hydrostatic) stresses are significantly larger than 5-10 *MPa* and the differential stresses are smaller than 35 *MPa*. Under such conditions one observes experimentally an isochoric creep process with only the first and second stages evidenced. As a result, in general, rock salt models, applicable for deepwater oil field developments, require only the consideration of the first and second creep stages and may approximate the deformation process as isochoric, see Fossum and Fredrich (2002) and Fredrich *et al.* (2007).

For deepwater applications, transient strain processes can be important. During drilling and oil production, stresses in the subsurface will change, leading to a transient creep. The strain contributions related to transient creep are in general significant for a time period on the order of tens of days. The relevance of the impact of the transient strains in the wellbore stability during drilling or long-term well integrity over the field lifetime depends upon the magnitude of the stress perturbations that are experienced. In addition, since the elastic yield stress for rock salt is very small, i.e., $\sigma_E < 1\,Mpa$, it's usual to model rock salt as a viscoplastic material with no yield criterion. Different models for rock salt have been proposed in the literature, see Aubertin *et al.* (1999) and Liang *et al.* (2007). Here, one uses the model presented by Yahya *et al.* (2000), and proposes a fully implicit algorithm using the Galerking finite element method, for the analysis of the behavior of rock salt under plane strain and axisymmetric conditions.

2. THE VISCOPLASTIC ROCK SALT MODEL WITH NO YIELD SURFACE

The model presented by Yahya *et al.* (2000) consider the following internal variables: the rest stresses χ_s and χ_l describing the short and long term effects of the kinematic hardening; the yield resistance stress R describing the isotropic hardening and the normalized (drag) stress K. These internal variables describe not only the strain hardening phenomenon but also the strain induced dynamic recovery and the thermal activated static recovery processes. Here, for simplicity, the problem is restricted to small displacements and deformations and the deformation process is assumed to

be isothermal. At this point, a total rest stress $\boldsymbol{\chi}$ is introduced and given by $\boldsymbol{\chi} = \boldsymbol{\chi}_s + \boldsymbol{\chi}_l$. The rock salt model proposed by Yahya *et al*. (2000) may be summarized by:

(i) The additive decomposition of the total strain into an elastic part, $\boldsymbol{\varepsilon}^e$, and a viscoplastic part, $\boldsymbol{\varepsilon}^c$, as

$$\boldsymbol{\varepsilon} = \boldsymbol{\varepsilon}^e + \boldsymbol{\varepsilon}^c \tag{1}$$

(ii) The stress versus elastic strain constitutive equation

$$\boldsymbol{\sigma} = \boldsymbol{D}\boldsymbol{\varepsilon}^e \tag{2}$$

in which

$$D_{ijrs} = G\left(\delta_{ir}\delta_{js} + \delta_{is}\delta_{jr}\right) + \bar{\lambda}\delta_{ij}\delta_{rs}, \tag{3}$$

where $G = \frac{E}{2(1+\nu)}$ (shear modulus) and $\bar{\lambda} = \frac{\nu E}{(1+\nu)(1-2\nu)}$ (Lamé's constant) with E denoting the Young's modulus and ν the Poisson's ratio.

(iii) The viscoplastic flow rule

$$\dot{\boldsymbol{\varepsilon}}^c = \dot{\lambda}\boldsymbol{N} \tag{4}$$

where

$$\boldsymbol{N} = \frac{3}{2}\frac{\left(\boldsymbol{\sigma}^D - \boldsymbol{\chi}^D\right)}{q} \tag{5}$$

and

$$\dot{\lambda} = \dot{e}^c_{ef} = a\left\langle\frac{q-R}{K}\right\rangle^N \tag{6}$$

with $\boldsymbol{\sigma} = \boldsymbol{\sigma}^D + p\boldsymbol{I}$, $\boldsymbol{\sigma}^D$ denoting the deviatoric stress, $p = \frac{1}{3}tr\left(\boldsymbol{\sigma}\right)$ the mean (hydrostatic) stress and $q = \sqrt{\frac{3}{2}\left(\boldsymbol{\sigma}^D - \boldsymbol{\chi}^D\right).\left(\boldsymbol{\sigma}^D - \boldsymbol{\chi}^D\right)}$ the effective von Mises stress measure. Here, a and N are material parameters that must be identified, $\dot{\lambda}$ denotes the rate of the viscoplastic multiplier and $\dot{e}^c_{ef}$ denotes the rate of the effective strain measure.

(iv) The evolution laws for the short and long term rest stresses

$$\dot{\boldsymbol{\chi}}^D_s = a_{1s}\left\{\frac{2}{3}\dot{\boldsymbol{\varepsilon}}^c - \boldsymbol{\chi}^D_s\frac{\dot{e}^c_{ef}}{\chi^\infty_{s_{ef}}}\right\} - \frac{a_{2s}}{\chi_{s_{ef}}}\left\langle\frac{\chi_{s_{ef}} - \chi^\infty_{s_{ef}}}{C}\right\rangle^q\boldsymbol{\chi}^D_s \tag{7}$$

and

$$\dot{\boldsymbol{\chi}}^D_l = a_{1l}\left\{\frac{2}{3}\dot{\boldsymbol{\varepsilon}}^c - \boldsymbol{\chi}^D_l\frac{\dot{e}^c_{ef}}{\chi^\infty_{l_{ef}}}\right\} - \frac{a_{2l}}{\chi_{l_{ef}}}\left\langle\frac{\chi_{l_{ef}} - \chi^\infty_{l_{ef}}}{C}\right\rangle^q\boldsymbol{\chi}^D_l \tag{8}$$

where $\chi_{l_{ef}} = \left[\frac{3}{2}\boldsymbol{\chi}^D_l.\boldsymbol{\chi}^D_l\right]^{\frac{1}{2}}$ and $\chi_{s_{ef}} = \left[\frac{3}{2}\boldsymbol{\chi}^D_s.\boldsymbol{\chi}^D_s\right]^{\frac{1}{2}}$ in which a_{1s}, a_{2s}, a_{1l}, a_{2l}, q and C are material parameters.

(v) The evolution laws for the yield resistance and drag stresses

$$\dot{R} = a_3\left(1-\frac{R}{R^\infty}\right)\dot{e}^c_{ef} - a_4\left\langle\frac{R-R^\infty}{C}\right\rangle^p \tag{9}$$

and

$$\dot{K} = a_5\left(1-\frac{K}{K^\infty}\right)\dot{e}^c_{ef} - a_6\left\langle\frac{K-K^\infty}{C}\right\rangle^u \tag{10}$$

in which a_3, a_4, a_5, a_6, p, and u are material parameters. The remaining variables, $\left\{\sigma^\infty_{vm}, \chi^\infty_{s_{ef}}, \chi^\infty_{l_{ef}}, R^\infty, K^\infty\right\}$, are named as the saturation or activation threshold and are defined by

$$\sigma^\infty_{vm} = \sigma_o \sinh^{-1}\left[\left(\frac{\dot{e}^c_{ef}}{\dot{e}^c_o}\right)^{\frac{1}{n}}\right], \quad \chi^\infty_{s_{ef}} = b_{os}\left(\frac{\sigma^\infty_{vm}}{\sigma_o}\right)^m, \quad \chi^\infty_{l_{ef}} = b_{ol}\left(\frac{\sigma^\infty_{vm}}{\sigma_o}\right)^m, \quad R^\infty = R_o\left(\frac{\sigma^\infty_{vm}}{\sigma_o}\right)^m \tag{11}$$

and

$$K^\infty = \frac{\left\langle\sigma^\infty_{vm} - \left(\chi^\infty + R^\infty\right)\right\rangle}{\left(\frac{\dot{e}^c_{ef}}{a}\right)^{\frac{1}{N}}}. \tag{12}$$

Here, σ_o, $\dot{e}^c_o$, n, m, b_{os}, b_{ol} and R_o are material parameters and $\langle x\rangle = \frac{1}{2}\left(x+|x|\right)$ denote the MacCauley parenthesis. The above saturation or activation thresholds are responsible for controlling the thermally activation of the static recovery processes.

3. DISCRETIZATION OF THE ROCK SALT MODEL

In order to derive the fully implicit algorithm, one assumes the solution to be known in the interval $\left[0, t_n\right]$ and imposes the equilibrium condition at t_{n+1}. As a result, one derives the following weak form: Determine $\vec{u}_{n+1} \in \mathbf{K}$ so that

$$\int_\Omega \boldsymbol{\sigma}_{n+1}.\boldsymbol{\varepsilon}\left(\vec{w}\right)\, d\Omega = \int_{\Gamma_t}\vec{t}_{n+1}.\vec{w}\, d\Gamma + \int_\Omega \rho\vec{b}_{n+1}.\vec{w}\, d\Omega, \forall\vec{w}\in \mathrm{V_u}\,. \tag{13}$$

in which $\mathbf{K}$ represents the set of admissible displacements and $\mathbf{V}_u$ the set of admissible variations.

3.1. Operator Split Algorithm

Here, in order to improve the robustness of the algorithm, one applies the operator split strategy, see Souza Neto *et al.* (2008), described by:

(i) The trial elastic step problem, formulated as: Given the strain history $\{\boldsymbol{\varepsilon}(t)\} \in [t_n, t_{n+1}]$, find $\boldsymbol{\varepsilon}^{e\,trial}_{n+1}$ and $\boldsymbol{\omega}^{trial}_{n+1}$, with $\boldsymbol{\omega}^{trial}_{n+1} \equiv (\boldsymbol{\varepsilon}^{c\,trial}_{n+1}, R^{trial}_{n+1}, K^{trial}_{n+1}, e^{c\,trial}_{ef_{n+1}}, \boldsymbol{\chi}^{D\,trial}_{s_{n+1}}, \boldsymbol{\chi}^{D\,trial}_{l_{n+1}})$, so that $\dot{\boldsymbol{\varepsilon}}^{e\,trial} = \dot{\boldsymbol{\varepsilon}}$ and $\dot{\boldsymbol{\omega}}^{trial} = 0$. As a result, one derives

$$\boldsymbol{\varepsilon}^{e^{trial}}_{n+1} = \boldsymbol{\varepsilon}_{n+1} - \boldsymbol{\varepsilon}^c_n \quad \text{and} \quad \boldsymbol{\omega}^{trial}_{n+1} = \boldsymbol{\omega}_n\,. \tag{14}$$

Once $\boldsymbol{\varepsilon}^{e^{trial}}_{n+1}$ is determined, one computes $e^{e\,trial}_{H_{n+1}} = \frac{1}{3}tr\left[\boldsymbol{\varepsilon}^{e^{trial}}_{n+1}\right]$, $\boldsymbol{\varepsilon}^{e\,D\,trial}_{n+1} = \boldsymbol{\varepsilon}^{e\,trial}_{n+1} - e^{e\,trial}_{H_{n+1}}\mathbf{I}$ and the trial elastic stresses $p^{trial}_{n+1} = \frac{E}{(1-2\nu)}e^{e\,trial}_{H_{n+1}}$ and $\overset{\cdot}{\boldsymbol{\sigma}}{}^{D\,trial}_{n+1} = 2G\boldsymbol{\varepsilon}^{e\,D\,trial}_{n+1}$.

(ii) The viscoplastic return mapping step problem

Here, by applying the fully implicit Euler method and performing some additional algebra, one derives the following coupled nonlinear problem, stated as: Given $\boldsymbol{\varepsilon}_{n+1}$, determine $\boldsymbol{\varpi} = \left(R_{n+1}, K_{n+1}, \boldsymbol{\chi}^D_{s_{n+1}}, \boldsymbol{\chi}^D_{l_{n+1}}, \boldsymbol{\sigma}^D_{n+1}\right)$ that satisfies:

$$R_1(\boldsymbol{\varpi}) = R_{n+1} - R_n - a_3\left(1-\frac{R_{n+1}}{R^{\infty}_{n+1}}\right)\Delta\, e^{c}_{ef_{n+1}} + a_4\left\langle\frac{R_{n+1}-R^{\infty}_{n+1}}{C}\right\rangle^{p}\Delta\, t = 0 \tag{15}$$

$$R_2(\boldsymbol{\varpi}) = K_{n+1} - K_n - a_5\left(1-\frac{K_{n+1}}{K^{\infty}_{n+1}}\right)\Delta\, e^{c}_{ef_{n+1}} + a_6\left\langle\frac{K_{n+1}-K^{\infty}_{n+1}}{C}\right\rangle^{u}\Delta\, t = 0 \tag{16}$$

$$R_3(\boldsymbol{\varpi}) = \boldsymbol{\sigma}^{D}_{n+1} + \frac{3G\,\Delta\, e^{c}_{ef_{n+1}}}{q_{n+1}}\left(\boldsymbol{\sigma}^{D}_{n+1} - \boldsymbol{\chi}^{D}_{n+1}\right) - \boldsymbol{\sigma}^{D\,trial}_{n+1} = 0 \tag{17}$$

$$R_4(\boldsymbol{\varpi}) = \boldsymbol{\chi}^{D}_{s_{n+1}} - \boldsymbol{\chi}^{D}_{s_n} - a_{1s}\left\{\frac{2}{3}\Delta\,\boldsymbol{\varepsilon}^{c}_{n+1} - \boldsymbol{\chi}^{D}_{s_{n+1}}\frac{\Delta\, e^{c}_{ef_{n+1}}}{\chi^{\infty}_{s_{ef_{n+1}}}}\right\} + \frac{a_{2s}\;\Delta\, t}{\chi_{s_{ef_{n+1}}}}\left\langle\frac{\chi_{s_{ef_{n+1}}}-\chi^{\infty}_{s_{ef_{n+1}}}}{C}\right\rangle^{q}\boldsymbol{\chi}^{D}_{s_{n+1}} = 0 \tag{18}$$

$$R_5(\boldsymbol{\varpi}) = \boldsymbol{\chi}^{D}_{l_{n+1}} - \boldsymbol{\chi}^{D}_{l_n} - a_{1l}\left\{\frac{2}{3}\Delta\,\boldsymbol{\varepsilon}^{c}_{n+1} - \boldsymbol{\chi}^{D}_{l_{n+1}}\frac{\Delta\, e^{c}_{ef_{n+1}}}{\chi^{\infty}_{l_{ef_{n+1}}}}\right\} + \frac{a_{2l}\;\Delta\, t}{\chi_{l_{ef_{n+1}}}}\left\langle\frac{\chi_{l_{ef_{n+1}}}-\chi^{\infty}_{l_{ef_{n+1}}}}{C}\right\rangle^{q}\boldsymbol{\chi}^{D}_{l_{n+1}} = 0 \tag{19}$$

in which $\boldsymbol{\chi}^{D}_{n+1} = \boldsymbol{\chi}^{D}_{s_{n+1}} + \boldsymbol{\chi}^{D}_{l_{n+1}}$, $\boldsymbol{\chi}^{D}_{n+1}$ denoting the deviator part of the total rest stresses, $\Delta\, e^{c}_{ef_{n+1}} = a\left\langle\frac{q_{n+1}-R_{n+1}}{K_{n+1}}\right\rangle^{N}\Delta\, t$, $\Delta\boldsymbol{\varepsilon}^{c}_{n+1} = \boldsymbol{\varepsilon}^{c}_{n+1} - \boldsymbol{\varepsilon}^{c}_{n}$ and $\Delta\, t = t_{n+1} - t_n$.

Once determined the set of internal variables, $\boldsymbol{\varpi} = \left(R_{n+1}, K_{n+1}, \boldsymbol{\chi}^{D}_{s_{n+1}}, \boldsymbol{\chi}^{D}_{l_{n+1}}, \boldsymbol{\sigma}^{D}_{n+1}\right)$, one may compute the Cauchy stress as

$$\boldsymbol{\sigma}_{n+1} = \boldsymbol{\sigma}^{D}_{n+1} + p_{n+1}\mathbf{I} \tag{20}$$

where

$$p_{n+1} = \frac{E}{(1-2\nu)}e^{e\,trial}_{H_{n+1}},\quad e^{e\,trial}_{H_{n+1}} = \frac{1}{3}tr\left(\boldsymbol{\varepsilon}^{e\,trial}_{n+1}\right) \text{ and } \boldsymbol{\varepsilon}^{e\,trial}_{n+1} = \boldsymbol{\varepsilon}_{n+1} - \boldsymbol{\varepsilon}^{c}_{n}. \tag{21}$$

The saturation or activation variables evaluated at t_{n+1} are given by

$$\sigma^{\infty}_{vm_{n+1}} = \sigma_o \sinh^{-1}\left[\left(\frac{\Delta\, e^{c}_{ef_{n+1}}}{\dot{e}^{c}_{o}\,\Delta\, t}\right)^{\frac{1}{n}}\right],\quad \chi^{\infty}_{s_{efn+1}} = b_{os}\left(\frac{\sigma^{\infty}_{vm_{n+1}}}{\sigma_o}\right)^{m}, \tag{22}$$

$$\chi^{\infty}_{l_{ef_{n+1}}} = b_{ol}\left(\frac{\sigma^{\infty}_{vm_{n+1}}}{\sigma_o}\right)^{m},\quad R^{\infty}_{n+1} = R_o\left(\frac{\sigma^{\infty}_{vm_{n+1}}}{\sigma_o}\right)^{m}, \text{ and } K^{\infty}_{n+1} = \frac{\left\langle\sigma^{\infty}_{vm_{n+1}} - \left(\chi^{\infty}_{n+1} + R^{\infty}_{n+1}\right)\right\rangle}{\left(\frac{\Delta\, e^{c}_{ef_{n+1}}}{a\,\Delta\, t}\right)^{\frac{1}{N}}} \tag{23}$$

with $\chi^{\infty}_{n+1} = \chi^{\infty}_{s_{efn+1}} + \chi^{\infty}_{l_{ef_{n+1}}}$. In order to solve the coupled set of non linear equation one employs Newton's method.

3.2. Incremental weak formulation of the problem

Once defined the constitutive model, one may solve the global equilibrium problem by employing an incremental procedure. The incremental formulation between t_n and t_{n+1} considers that

$$\vec{u}_{n+1} = \vec{u}_n + \Delta\,\vec{u}_n \tag{24}$$

so that, at time t_{n+1}, the weak formulation of the problem may be stated as: Determine $\vec{u}_{n+1} \in \mathbf{K}$, which solves

$$F_1\left(\vec{u}_{n+1};\vec{w}\right) = \int_{\Omega}\boldsymbol{\sigma}_{n+1}.\boldsymbol{\varepsilon}\left(\vec{w}\right)\, d\Omega - \int_{\Omega}\rho\,\vec{b}_{n+1}.\vec{w}\,d\Omega - \int_{\Gamma^{t}}\vec{t}_{n+1}.\vec{w}\, dA = 0,\quad \forall\vec{w}\in\mathbf{V}_{\boldsymbol{u}} \tag{25}$$

Since the above problem is non-linear, one applies Newton's method leading to the solution of a sequence of linearized problems.

Consistent linearization procedure

Let $\vec{u}_{n+1}^{k}$ be the estimate solution of (25) at the *k-th* iteration and consider that

$$\vec{u}_{n+1}^{k} = \vec{u}_{n} \text{ at } k = 0 . \tag{26}$$

For the *k-th* iteration of the solution procedure, one has

$$\vec{u}_{n+1}^{k+1} = \vec{u}_{n+1}^{k} + \Delta\vec{u}_{n+1}^{k} . \tag{27}$$

The determination of the increment $\Delta\vec{u}_{n+1}^{k}$ is obtained by imposing

$$F_1\left(\vec{u}_{n+1}^{k} + \Delta\vec{u}_{n+1}^{k}; \vec{w}\right) = 0, \quad \forall \vec{w} \in \mathbf{V}_{\boldsymbol{u}} . \tag{28}$$

Considering $F_1(\circ)$ being Gateaux differentiable one derives the first order approximation given by

$$F_1\left(\vec{u}_{n+1}^{k} + \Delta\vec{u}_{n+1}^{k}; \vec{w}\right) \simeq F_1\left(\vec{u}_{n+1}^{k}; \vec{w}\right) + DF_1\left(\vec{u}_{n+1}^{k}; \vec{w}\right)\left[\Delta\vec{u}_{n+1}^{k}\right] . \tag{29}$$

Now, replacing (29) into (28) finally yields

$$DF_1\left(\vec{u}_{n+1}^{k}; \vec{w}\right)\left[\Delta\vec{u}_{n+1}^{k}\right] = -F_1\left(\vec{u}_{n+1}^{k}; \vec{w}\right) \tag{30}$$

where

$$DF_1\left(\vec{u}_{n+1}^{k}; \vec{w}\right)\left[\Delta\vec{u}_{n+1}^{k}\right] = \lim_{\varepsilon \to 0} \frac{F_1\left(\vec{u}_{n+1}^{k} + \varepsilon\Delta\vec{u}_{n+1}^{k}; \vec{w}\right) - F_1\left(\vec{u}_{n+1}^{k}; \vec{w}\right)}{\varepsilon} = \frac{d}{d\varepsilon}\left[F_1\left(\vec{u}_{n+1}^{k} + \varepsilon\Delta\vec{u}_{n+1}^{k}; \vec{w}\right)\right]_{\varepsilon=0} . \tag{31}$$

Since Ω is fixed and the prescribed traction and body forces are assumed to be independent of the displacement field, one derives

$$DF_1\left(\vec{u}_{n+1}^{k}; \vec{w}\right)\left[\Delta\vec{u}_{n+1}^{k}\right] = \int_{\Omega} \frac{d}{d\varepsilon}\left[\boldsymbol{\sigma}_{n+1}\left(\boldsymbol{\varepsilon}\left(\vec{u}_{n+1}^{k}\right)\right)\right]_{\varepsilon=0} . \boldsymbol{\varepsilon}\left(\vec{w}\right)\, d\Omega = \int_{\Omega}\left[D_T\left(\vec{u}_{n+1}^{k}\right)\right]_{ijkl} \varepsilon_{kl}\left(\Delta\vec{u}_{n+1}^{k}\right) . \varepsilon_{ij}\left(\vec{w}\right)\, d\Omega \tag{32}$$

in which $\left[D_T\left(\vec{u}_{n+1}^{k}\right)\right]_{ijkl} = \frac{\partial\sigma_{ij}}{\partial\varepsilon_{kl}}\left(\vec{u}_{n+1}^{k}\right)$ is the consistent tangent modulus.

3.3. Determination of the consistent tangent modulus

The consistent tangent operator is given by

$$\left[\mathbf{D_T}\right]_{ijkl} = \frac{\partial\boldsymbol{\sigma}_{ij}}{\partial\boldsymbol{\varepsilon}_{kl}} = \frac{\partial\boldsymbol{\sigma}_{ij}}{\partial\boldsymbol{\varepsilon}_{kl}^{e^{trial}}} \tag{33}$$

However, since $\sigma_{ij} = \sigma_{ij}^{D} + p\delta_{ij}$, one derives

$$\left[D_T\right]_{ijkl} = \frac{\partial\sigma_{ij}^{D}}{\partial\varepsilon_{kl}^{e^{trial}}} + \frac{\partial p}{\partial\varepsilon_{kl}^{e^{trial}}}\delta_{ij} \text{ with } \frac{\partial p}{\partial\varepsilon_{kl}^{e^{trial}}} = \frac{E}{3(1-2\nu)}\delta_{kl} . \tag{34}$$

In order to compute $\frac{\partial\sigma_{ij}^{D}}{\partial\varepsilon_{kl}^{e^{trial}}}$ one notice that the solution of (15-19), given by $\boldsymbol{\varpi}$ is obtained for a given value of $\boldsymbol{\varepsilon}_{n+1}$.

However, $\boldsymbol{\varepsilon}_{n+1}^{e^{trial}} = \boldsymbol{\varepsilon}_{n+1} - \boldsymbol{\varepsilon}_{n}^{c}$ and $\boldsymbol{\varepsilon}_{n}^{c}$ is a constant, at t_{n+1}, which allow us to conclude that $\boldsymbol{\varpi} = \boldsymbol{\varpi}\left(\boldsymbol{\varepsilon}_{n+1}^{e^{trial}}\right)$, i.e.,

$$R_{n+1} = R_{n+1}\left(\boldsymbol{\varepsilon}^{e^{trial}}_{n+1}\right) \tag{35}$$

$$K_{n+1} = K_{n+1}\left(\boldsymbol{\varepsilon}^{e^{trial}}_{n+1}\right)$$

$$\boldsymbol{\sigma}^{D}_{n+1} = \boldsymbol{\sigma}^{D}_{n+1}\left(\boldsymbol{\varepsilon}^{e^{trial}}_{n+1}\right)$$

$$\boldsymbol{\chi}^{D}_{s_{n+1}} = \boldsymbol{\chi}^{D}_{s_{n+1}}\left(\boldsymbol{\varepsilon}^{e^{trial}}_{n+1}\right)$$

and

$$\boldsymbol{\chi}^{D}_{l_{n+1}} = \boldsymbol{\chi}^{D}_{l_{n+1}}\left(\boldsymbol{\varepsilon}^{e^{trial}}_{n+1}\right)$$

As a result, differentiating (35) with respect to $\boldsymbol{\varepsilon}^{e^{trial}}_{n+1}$ leads to a linear system of equations that may be solved for $\frac{\partial \boldsymbol{\sigma}^{D}_{n+1}}{\partial \varepsilon^{e^{trial}}_{kl}}$.

4. NUMERICAL EXAMPLES

The discretization of the problem is obtained by the application of the Galerkin Finite Element method using a Tri 6 element. In order to verify the adequacy of the model and the proposed implicit algorithm, one solves a set of simple problems. The parameters used in these examples are given in "Table 1". And the experimental data was extracted from the work of Yahya *et al*. (2000), relative to the rock salt properties of Avery Island.

Table 1. Parameters employed by the model

$E = 31\ GPa$	$\nu = 0.38$	$A = 0.176\times10^{-05}\ s^{-1}$
$A_{l_s} = 20.395\ GPa$	$A_{l_l} = 1218\ MPa$	$A_{2_s} = 0.104\times10^{-02}\ MPas^{-1}$
$A_{2_l} = 0.458\times10^{-15}\ MPas^{-1}$	$A_3 = 95\ MPa$	$A_4 = 0.456\times10^{-08}\ MPas^{-1}$
$A_5 = 27\ MPa$	$A_6 = 0.543\times10^{-13}\ MPas^{-1}$	$B_{o_s} = 1.47\ MPa$
$B_{o_l} = 3.37\ MPa$	$R_o = 3.04\ MPa$	$\boldsymbol{\sigma}_o = 9.15\ MPa$
$\dot{\boldsymbol{\varepsilon}}_o = 0.135\times10^{-10}\ s^{-1}$	$N = 4$	$n = 3$
$m = 1$	$C = 1.0\ MPa$	$p = 2$
$u = 2$	$q = 2$	$K_o = 1.0\ MPa$

4.1. Triaxial compression

Here, in order to validate the proposed algorithm, one compares the computed numerical solution for two loading cases with the experimental data obtained for the rock salt in Avery Island. In the first simulation, a rock salt specimen is subjected to a prescribed displacement, as depicted in Figure 1. The prescribed displacement is applied by a linear ramp with a strain rate of $8.7\times10^{-6}\ s^{-1}$ up to the value of $\bar{u} = -2.12$ mm. The specimen is confined by a lateral pressure of $15MPa$. The second simulation considers the same test but with a strain rate of $8.3\times10^{-08}\ s^{-1}$ and a maximum displacement of $\bar{u} = -2.0$ mm. The problem is considered to be axisymmetric and were applied respectively 1000 and 7000 displacement increments.

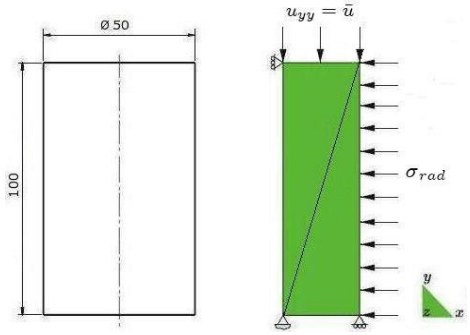

Fig. 1 – Definition of the problem

The stress-strain curves obtained numerically and the experimental data, obtained in Yahya *et al*. (2000), for both simulations are depicted in Figure 2. The stress measure used in Figure 2 is the stress difference, defined as the difference between the axial and the confining lateral pressure, given by $\Delta\sigma = \sigma_{ax} - \sigma_{rad}$.

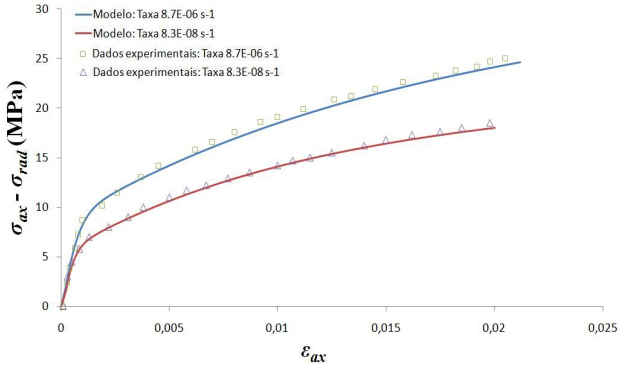

Fig. 2 – Stress difference versus axial strain curve for both simulations

4.2. Creeping test resulting from a triaxial compression

Here, one considers a triaxial compression creep test that takes place for three different constant axial stress loadings. The rock salt specimen is subjected to a confining lateral stress and subjected to a constant axial stress $\bar{\sigma}$, as depicted in Figure 3.

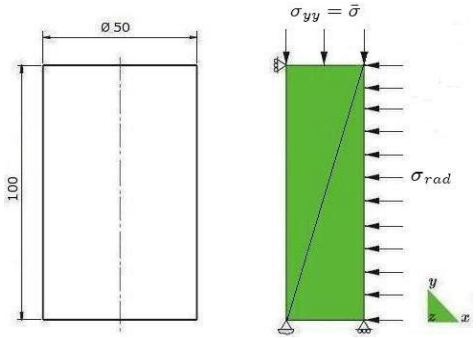

Fig.3 – Definition of the triaxial creeping test

The problem is considered to be axisymmetric and the loading to be applied for 48 hours. The loading cases considered here are: (1) $\bar{\sigma} = 10$ MPa with $\sigma_{rad} = 5$ MPa; (2) $\bar{\sigma} = 20$ MPa with $\sigma_{rad} = 10$ MPa; and $\bar{\sigma} = 20$ MPa with $\sigma_{rad} = 5$ MPa. Figure 4 shows the evolution of the total axial strain as a function of time for the three different loading cases, expressed in term of their stress difference, $\Delta\sigma$, level.

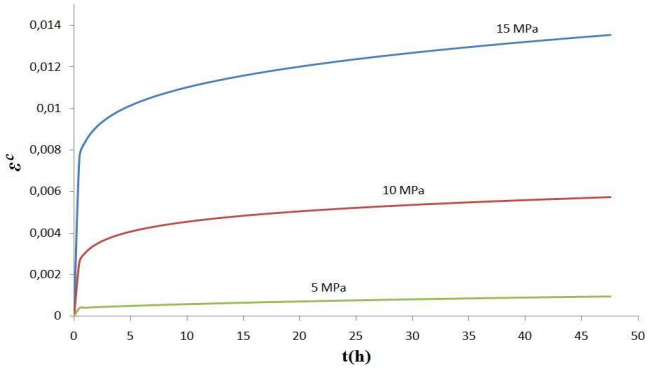

Fig. 4 – Evolution of the axial strain for the three stress difference loading cases

4.3. Stress relaxation test

Here, one considers a stress relaxation test that takes place for three different prescribed constant axial strains. The rock salt specimen is subjected to a confining lateral stress and subjected to a prescribed axial strain $\bar{\boldsymbol{\varepsilon}}_{ax}$, as depicted in Figure 5.

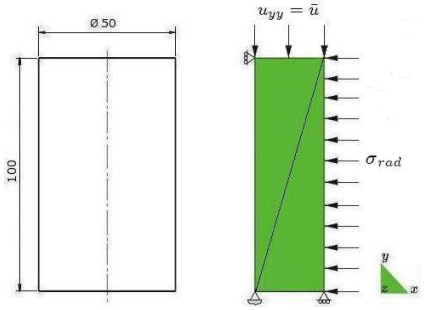

Fig. 5 – Description of the triaxial compression stress relaxation test

The problem is considered to be axisymmetric and the prescribed constant strain loading to be applied for 24 hours, as depicted in Figure 6. Three prescribed strain loadings were obtained by prescribing the following displacements: (1) case $\bar{u} = -0,4mm$; (2) case $\bar{u} = -0,3mm$; and (3) case $\bar{u} = -0,2mm$. The confining pressure for all three loading cases is given by 5 Mpa and the total loading time considered is of 24 hours.

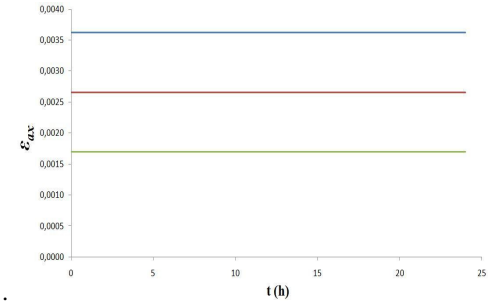

Fig. 6 – Prescribed strain loading for the stress relaxation tests

Figure 7 depicts the time evolution of the stress difference for the three stress relaxation tests, for 24 hours.

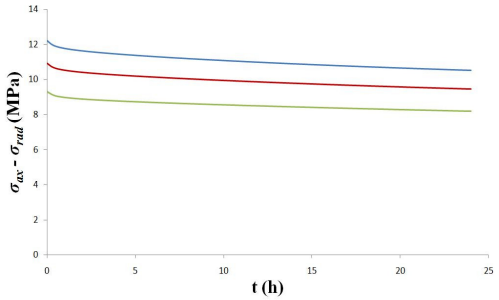

Fig. 7 – Time evolution of the stress difference for the three stress relaxation tests

4.4. Diametrical compression test

Here, one considers a diametrical compression test of a rock salt specimen, as depicted in Figure 8. The specimen is subjected to a plane strain condition and due to the symmetry conditions only one fourth of the domain is modeled. The specimen is subjected to a prescribed displacement applied by a linear ramp with a maximum displacement of $\bar{u} = -0.5mm$.

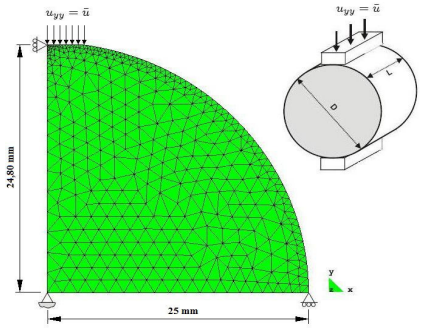

Fig. 8 – Description of the diametrical compression test

The mesh consists in 742 elements and 1603 nodes and the analysis employed 2000 displacement increments in the "loading process". Figure 9 shows the distribution of the level sets representing the displacement component, u_x at the end of the analysis.

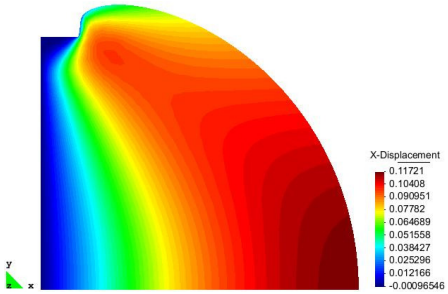

Fig. 9 – Distribution of the level sets of the displacement component u_x

Figure 10 shows the distribution of the level sets representing the displacement component, u_y at the end of the analysis.

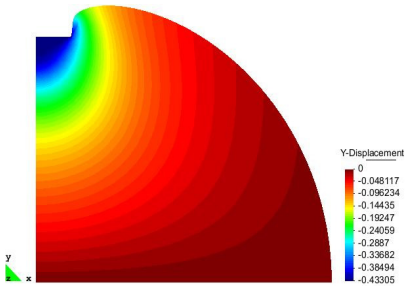

Fig. 10 – Distribution of the level sets of the displacement component u_y

Figure 11 shows the distribution of the level sets representing the stress component, σ_{xx}, at the end of the analysis.

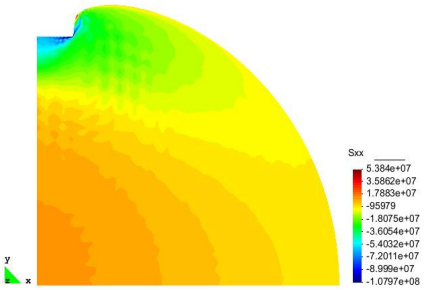

Fig. 11 - Distribution of the level sets of the stress component σ_{xx}

Figure 12 shows the distribution of the level sets representing the stress component, σ_{xy}, at the end of the analysis.

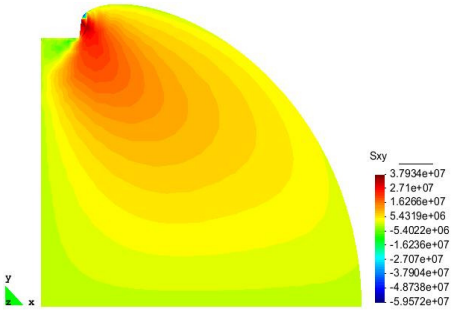

Fig. 12 - Distribution of the level sets of the stress component σ_{xy}

5. CONCLUSIONS

The proposed implicit numerical scheme made use of the fully implicit Euler method and have shown to be robust in solving the proposed examples. The validation of the algorithm was obtained by comparing the numerical solutions with the available experimental data, which has shown to be in a good agreement.

The problem illustrated in Figure 8 is a simplified model of an experimental diametrical compression test. The proper modeling of such tests requires the usage of unilateral displacement constraint at the loading surface. Due to the simplified modeling one can see a large plastic flow of the rock salt in the neighborhood of the loading surface. The oscillations in the boundary of the level sets in Fig. 11 can be reduced significantly by using a more refined finite element mesh.

The rock salt model considered in this paper showed to be adequate to describe a wide range of rock salt deformation processes and adequate for modeling rock salt behavior under complex loading conditions.

6. ACKNOWLEDGEMENTS

The support of the CNPq, Conselho Nacional de Desenvolvimento Científico e Tecnológico, of Brazil is gratefully acknowledged.

7. REFERENCES

Aubertin, M., Yahya O. M. L., & Julien, M., 1999. "Modeling mixed hardening of alkali halides with a modified version of an internal state variables model", International Journal of Plasticity, vol. 15, pp. 1067-1088.

Souza Neto, E.A., Peric D., Owens D., 2008. "Computational methods for plasticity: theory and applications", John Wiley & Sons Ltd.

Fossum A. F. and Fredrich J. T, 2002, "Salt Mechanics Primer for Near-Salt and Sub-Salt Deepwater Gulf of Mexico Field Developments", Report Sandia National Laboratories.

Fredrich, J.T., Fossum, A.F. and Hickman, R.J., 2007, "Mineralogy of deepwater Gulf of Mexico salt formations and implications for constitutive behavior", Journal of Petroleum Science and Engineering vol. 57, pp. 354-374.

Liang, W., Yang, C., Zhao, Y., Dusseault, M. B., & Liu, J., 2007. "Experimental investigation of mechanical properties of bedded salt rock", International Journal of Rock Mechanics and Mining Sciences vol. 44, pp. 400-411.

Yahya, O. M. L., Aubertin, M., & Julien, M. R. A, 2000. "Unified representation of the plasticity, creep and relaxation behavior of rock salt", International Journal of Rock Mechanics and Mining Sciences, vol. 37, pp. 787-800.

8. RESPONSIBILITY NOTICE

The authors are the only responsible for the printed material included in this paper.